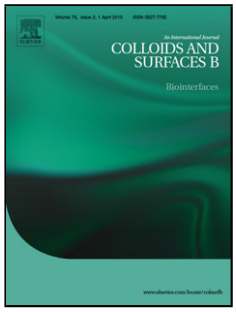

Title: Femtomolar oligonucleotide detection by a one-step gold nanoparticle-based assay

Author: Prayanka Rajendran Silvan Kaufmann János V*örös*
Marcy Zenobi-Wong László Demkó

PII: S0927-7765(15)30069-2
DOI: http://dx.doi.org/doi:10.1016/j.colsurfb.2015.07.035
Reference: COLSUB 7239

To appear in: *Colloids and Surfaces B: Biointerfaces*

Received date: 9-4-2015
Revised date: 20-6-2015
Accepted date: 13-7-2015

Please cite this article as: Prayanka Rajendran, Silvan Kaufmann, János V*ddotorddotos*, Marcy Zenobi-Wong, László Demkó, Femtomolar oligonucleotide detection by a one-step gold nanoparticle-based assay, *Colloids and Surfaces B: Biointerfaces* (2015), http://dx.doi.org/10.1016/j.colsurfb.2015.07.035

Femtomolar oligonucleotide detection by a one-step gold nanoparticle-based assay

Prayanka Rajendran[a], Silvan Kaufmann[a], János Vörös[a], Marcy Zenobi-Wong[b], László Demkó[a,*]

[a] *Laboratory of Biosensors and Bioelectronics, Institute for Biomedical Engineering, ETH Zurich, CH-8092 Zurich, Switzerland*
[b] *Cartilage Engineering and Regeneration, Department of Health Sciences and Technology, ETH Zurich, CH-8093 Zurich, Switzerland*

Abstract

A sequence-specific oligonucleotide detection method based on the tail-to-tail aggregation of functionalized gold nanoparticles in the presence of target analytes is presented together with its optimization and capabilities for detection of Single Nucleotide Polymorphisms (SNPs). In this single-step method, capture probes are freely accessible for hybridization, resulting in an improved assay performance compared to substrate-based assays. The analytes bring the nanoparticles close to each other via hybridization, causing a red shift of the nanoparticle plasmon peak detected by a spectrophotometer or CCD camera coupled to a darkfield imaging system. Optimal conditions for the assay were found to be i) use of capture probes complementary to the target without any gap, ii) maximum possible probe density on the gold nanoparticles, and iii) 1 M ionic strength buffer. The optimized assay has a 1 fM limit of detection and fM to 10 pM dynamic range, with detection of perfect match sequences being 3 orders of magnitude more sensitive than targets with single nucleotide mismatches.

Keywords: DNA sensing, femtomolar detection, oligonucleotide, gold nanoparticle, local surface plasmon resonance, biosensor

*corresponding author
Email address: demko@biomed.ee.ethz.ch (László Demkó)

1. Introduction

During the last decade, and especially since the completion of the Human Genome Project[1, 2], oligonucleotide sensing has grown exponentially to assist in the identification and characterization of the different DNA sequence variants, becoming a useful tool in genetics research[3]. The genetic information and its modifications (polymorphisms) are indispensable to understand the diversity found among humans and the genetic factors associated with human diseases[4–6]. These modifications involve insertions, deletions, and substitutions of one or more nucleotides from which single base substitution polymorphisms, also known as Single Nucleotide Polymorphisms (SNPs), occur the most frequently[7–9]. The genetic variability as a result of SNPs has been linked to several diseases such as cancer[10–12], diabetes[13], and obesity[14], revealing possible medical applications. However, due to the increasing demand for genetic analysis, rapid, highly scalable, and low-cost oligonucleotide sensors capable of SNP detection have to be developed.

Up to now conventional methods for selective oligonucleotide quantification are dominated by fluorescence-based technologies[15, 16] or indirect measurements using polymerase chain reaction (PCR) based detection techniques[17, 18]. In addition to the complex instrumentation needed, both the approaches have several limitations as well. Fluorescence detection has low stability due to photobleaching and low signal-to-noise ratio for the single events, while PCR detection is limited by high error rates of the replicating enzymes, difficulty in amplifying short sequences, and variable efficiency of the reverse transcription process[19–22]. As such it is difficult to compare different genes quantitatively. The 1–10 copy sensitivity level offered by PCR is highly dependent on the reaction mix as well as on other factors[23], and thus, PCR-less target DNA amplification methods have been developed to eliminate the drawbacks of PCR, reaching subattomolar sensitivity[24]. However, for typical applications where sub-picomolar detection is sufficient, the simplicity of direct oligonucleotide quantification assays makes them more attractive for various applications.

Optical detection methods based on the localized surface plasmon resonance of gold nanoparticles (AuNPs) provide such sensitivity[25]. The phenomenon, as a result of the collective oscillation of conduction electrons, is responsible for a pronounced scattering intensity of AuNPs. The resonance condition depends on their size, shape, as well as the refractive index conditions in their close vicinity, making it possible to detect even single binding events between functionalized nanoparticles[26, 27]. For functionalization, thiol-modified oligonucleotides can be attached to the surface of AuNPs by direct covalent bonding[28]. These DNA functionalized cost-effective nanoparticle constructs are used extensively for various biosensors[29–37] including SNP detection[38–41], as well as for gene delivery[42] and molecular imaging[43, 44]. In applications typical for oligonucleotide sensing the analyte induces the agglomeration of AuNPs by hybridization, resulting in a red shift of the nanoparticle plasmon peak[45].

In this study, we present a one-step assay and its optimization for AuNP based detection of short DNA targets in the sub-picomolar range. The schematics of the assay is shown in Fig. 1. 50 nm AuNPs are functionalized with thousands of capture DNA molecules specific to the analyte (target DNA). The binding of analytes half-complementary to each capture probe sequence pulls the nanoparticles close to each other (<10 nm[46]) and maintains their close proximity throughout the experiment. The formed aggregates change the plasmonic properties of the involved AuNPs, resulting in red shifted scattering spectra. The size of the AuNPs was chosen as a compromise between optical signature, available capture probes per AuNP, and AuNP stability in solution [33, 47]. The one-step assay happens in solution without any rinsing steps, in order to maximize the number of available capture probes and analytes. The spectral detection is based on the use of a darkfield microscope coupled to a spectrometer, which provided enhanced contrast to the AuNPs by producing a constant, almost perfectly black background necessary for the reliable detection of the spectral information. Apart from the proof-of-concept experiments, this paper also includes the optimization of the assay in terms of buffer ionic strength, length of unpaired region between the target DNA and capture probe (gap size), and den-

sity of capture DNAs on the AuNPs. The optimized assay with sub-picomolar sensitivity was used for SNP detection. Matching targets could be detected with 3 orders of magnitude more sensitivity compared to targets with a single base mismatch.

2. Experimental

2.1. Materials and reagents

Citrate capped AuNPs with 48 nm mean diameter, $< 8\%$ coefficient of variation, and 4.5×10^{10} colloids/ml concentration were purchased from BBI Solutions (Cardiff, UK), thiolated oligonucleotides from IBA GmbH (Göttingen, Germany), and target DNAs from Microsynth AG (Balgach, Switzerland). Tris(2-carboxyethyl)phosphine (TCEP), sodium dodecyl sulphate (SDS), glycerol, sodium chloride (NaCl), phosphate buffered saline (PBS), and HPLC grade ethanol were purchased from Sigma-Aldrich (Buchs, Switzerland), while Cobas Integra Cleaner from Roche Diagnostics (Basel, Switzerland). Polydimethylsiloxane (PDMS) was made from Sylgard 184 silicone elastomer kit purchased from Dow Corning (Midland, MI, USA). All aqueous solutions were made with purified Milli-Q water from an Elix 5 water purification system (Merck Millipore, Billerica, MA, USA). Prior to use all buffers used for AuNP functionalization and the assay were filtered with Minisart 0.2 μm filters purchased from Sigma-Aldrich (Buchs, Switzerland).

2.2. DNA sequences

Table 1 contains the capture probe and analyte sequences used in this study, following the work of Storhoff et al.[30] Capture probes are 22 bases long consisting of 12 bases complementary to either half of the target and a 10 bases long poly-A spacer tail to increase the hybridization efficiency to the target by increasing the accessibility of the capture probes[48]. Analytes are 24–28 bases long DNA molecules, comparable to the typical lengths of micro RNAs and short interfering RNAs of interest[49]. The nucleotide sequences were chosen in

a way that upon hybridization the target molecule assembles the AuNP "heads" and their capture probe "tails" in a tail-to-tail fashion (see Fig. 1) as opposed to head-to-head or head-to-tail configurations. Keeping the AuNPs further away from each other is expected to result in lower interparticle repulsion and more stable dimer formation[50].

name	**sequence**		
capture A	3′–SH–	A AAA AAA AAA ATG CTC AAC TCT	–5′
capture B	3′–	TAG GAC TTA CGC AAA AAA AAA A	–SH–5′
poly-A	3′–	A AAA AAA AAA	–SH–5′
target (T)	5′–	TAC GAG TTG AGA ATC CTG AAT GCG	–3′
T2bp	5′–	TAC GAG TTG AGA **GG** ATC CTG AAT GCG	–3′
T4bp	5′–	TAC GAG TTG AGA **GGGG** ATC CTG AAT GCG	–3′
T4bp1MM	5′–	TAC G**C**G TTG AGA **GGGG** ATC CTG AAT GCG	–3′

Table 1: Oligonucleotides used for the functionalization of AuNPs and as target DNA strands. SH denotes the thiol group, 2bp and 4bp the targets with a gap size of 2 and 4 bases, respectively, while 1MM and the underlined DNA nucleotide mark the target and corresponding mismatch for the SNP study.

2.3. Capture DNA functionalization to AuNPs

Prior to thiolated-DNA functionalization the protecting disulfide groups of the DNA sequences were reduced using a TCEP solution. A volume of 100 μM DNA dissolved in Milli-Q was mixed with TCEP (2 mM in 10 mM filtered PBS buffer at pH 8.5) at a ratio of 3:1 and incubated at room temperature for 90 min, resulting in a final thiol-modified DNA and TCEP concentration of 75 μM and 0.5 mM, respectively.

DNA–AuNPs were constructed by conjugating various sequences (capture probe A, capture probe B, and poly-A) to AuNPs in bulk by mixing 1 ml 75 pM AuNP solution with 66 μl of the aforementioned reduced thiol-modified DNA solution. 10 μl of the mixture was separated, centrifuged (20 min at 14500 rpm in an Eppendorf 5810 R centrifuge, Eppendorf AG, Hamburg, Germany), and the supernatant was collected for DNA quantification in a UV-Vis spectrophotometer

(NanoDrop 1000, NanoDrop Products, Wilmington, DE, USA). The mixture was then adjusted to 0.01% filtered SDS, sonicated for 10 s in order to increase the DNA loading[51], and incubated overnight. After incubation, filtered PBS at pH 7.4 was added to reach the phosphate concentration of 10 mM, and then the mixture was sonicated again for 10 s. Filtered NaCl in steps of 0.1 M per hour followed by 10 s of sonication was added until the maximum salt concentration of 1 M was reached. After each step of salt addition the color of the AuNP solution was checked, and whenever the solution changed color from pink to purple due to aggregation, the waiting time before the next step was doubled in order to allow more DNA binding before the next higher ionic strength step. The final mixture was incubated overnight, and then 10 μl was collected and centrifuged again for DNA quantification, just as before. As a last step, particle solutions were washed three times by centrifugation for 5 min at 14500 rpm, where the supernatant was replaced by 1 ml of Milli-Q water after the first two washing cycles and by 1 ml of hybridization buffer (10 mM PBS at pH 7.4 and 0.3 M or 1 M NaCl according to the salt study, filtered) after the third washing step.

The quantification of the DNA density on the AuNPs showed that the average number of capture probes per AuNP is independent of the sequence used, and as such, makes the comparison of the assay performances in the case of different sequences valid. See supporting information S1 for the details and further discussion on the results of the quantification.

2.4. Assay procedure

2.4.1. Substrate preparation

Microscope slides and coverslips (Menzel-Gläser, Gerhard Menzel GmbH, Braunschweig, Germany) were cleaned with particle free wipes using diluted Cobas Integra Cleaner (1:10 in Milli-Q), alternately rinsed 3× between ethanol and Milli-Q, and finally dried with nitrogen gas and stored in petri dishes in a laminar flow hood until further use. PDMS wells with a diameter of 2.5 mm were prepared by punching holes into sheets having the same height. Squares

with dimensions of $\sim 1 \times 1$ cm^2 containing individual holes were cut out and cleaned with Cobas Integra Cleaner (1:10 in Milli-Q) followed by rinsing with Milli-Q and ethanol three times, then left in a laminar flow hood to dry until further use.

2.4.2. Assay

Analyte solutions with concentrations ranging from 0.1 fM to 1 μM were aliquoted using the hybridization buffer. 5–5 μl of DNA-AuNP solutions containing capture probes A and B were mixed with 10 μl target solution, vortexed for 5 s (IKA Vortex Genius 3, IKA-Werke GmbH, Staufen, Germany), then subjected to a heat cycle on a Biometra T-personal Combi thermocycler (Biometra GmbH, Göttingen, Germany) consisting of a 5 min step at 75 °C and 10 min at 25 °C. After the heat cycle 20 μl glycerol buffer (30% glycerol dissolved in hybridization buffer then filtered) was added to reach the final solution of 11250 particles/nl (18.75 pM, including both A and B). Glycerol at a final concentration of 15% was used to prevent drying of the wells. In the laminar flow hood PDMS wells were mounted on microscope slides and were filled up with 10 μl solution after brief vortexing. Each well is then covered with coverslips and left overnight in a petri dish to allow the AuNPs to settle. The following day coverslips and PDMS wells were carefully removed and replaced by a clean coverslip for darkfield imaging. Error bars for dose-response curves (see data analysis below) were obtained from the standard deviation of measurements made on three separate wells from the same assay preparation.

2.5. Instrumentation and data analysis

2.5.1. Instrumentation

A hyperspectral nanoscale optical imaging system based on an Olympus BX53F microscope, an enhanced darkfield optical illumination system (NA=1.2–1.4, CytoViva Inc., Auburn, AL, USA), a 60× oil immersion objective (Olympus UPlanFLN 60×/1.25 Oil Iris), a Specim V10E imaging spectrograph (Specim, Oulu, Finland), and a pco.pixelfly CCD camera (PCO AG, Kelheim, Germany)

was used for image acquisition in transmission mode. The frame size of each scan was 150 μm $\times$ 150 μm consisting of 696 lines, and at the beginning of the experiments the acquisition time for measuring the spectral information was set to 0.015 s per line in order to have the scattering intensity of samples with the highest target concentration (i.e. with the highest level of aggregation and thus with the highest intensity) at around 80% of the detection limit. Representative color (RGB) images were generated by using the spectral intensity values at 641, 550, and 459 nm as red, green, and blue channels, respectively.

2.5.2. Data analysis

The pixels of the dark field images represent the AuNPs, single or aggregated, and the background. Since the intensity and partially the spectral shape of background pixels can change due to fluctuations in the intensity of the illumination, instrumental noise can be reduced by identifying and removing these pixels from the spectral analysis. Pixels having their maximum spectral intensity (i.e. the highest value within the spectrum) lower than 1% of the detection limit were considered background pixels. The intensity values of the remaining pixels were then averaged together at each wavelength to calculate the raw spectrum of the images. The resulting raw spectrum similar to the one depicted in Fig. 2 (black curve) still contains a signal component representing the dark current of the detector, a baseline constant for all the wavelengths but fluctuating over time, which was approximated and removed by fitting an exponential function (green dashed curve) to the raw spectrum above 800 nm. The resulting real spectrum (red curve) was then analyzed by fitting a second-order polynomial function (blue continuous curve) to the maximum and its 30 nm vicinity of the curve to determine the maximum position and maximum value, and from this peak value the full width at half maximum (FWHM) of the spectrum. Dose-response curves were calculated from these spectral properties and were fitted by sigmoidal curves. The equilibrium dissociation constant K was estimated by the analyte concentration value corresponding to the inflection point of the fits.

3. Results and discussion

3.1. Darkfield assay images

Fig. 3 shows typical darkfield images of AuNPs at various aggregation levels. Single AuNPs with 50 nm diameter have their plasmon peak at 535 nm, and as such are represented by green pixels. The few yellowish pixels of Fig. 3a are due to a small number of aggregates that formed spontaneously. The level of this unspecific aggregation depends on the age of the nanoparticle batch and changes slightly over time. Thus, samples corresponding to the same dose-response curve were prepared at the same time using the same batch of nanoparticles. Upon increasing analyte concentrations the level of aggregation increases, and pairs as well as bigger aggregates start to form, as indicated by the yellowish pixels resulting from the red-shifted plasmon peak of the corresponding AuNPs (see Fig. 3b-c).

3.2. Spectral analysis

The trend of red-shifting of the spectra can be followed in Fig. 4a showing the results of a set of experiments studying the dose-response curve in the case of the optimized assay (see the next sections for details). Simultaneously with the red shift of the peak position, the peak amplitude also increases be cause the aggregates have bigger scattering cross-sections resulting in higher scattering intensities compared to that of the single particles. Fig. 4b plots the most important parameters calculated from the spectra depicted in Fig. 4a, i.e. the maximum position, maximum value, FWHM, and the ratio of the intensity values measured at wavelengths corresponding to the red and green channels (r/g, see arrows in Fig. 4a), as functions of the analyte concentration. Even though the peak amplitude is increasing towards higher concentrations, it has a low signal-to-noise ratio compared to those of the other properties. Changes in the peak position and r/g ratio can be scaled together and show an upturn in the pM range, but measuring the FWHM gives a sharper change in the same concentration range and a lower limit of detection (LOD, calculated from the

zero target value plus 3 times its standard deviation). Based on the optimized assay, the LOD is 1 fM for the FWHM values, represented by the shaded area in Fig. 4b (see supporting information S2 for a close-up look). While the FWHM seems to be the most sensitive indicator for the analyte concentration changes, its calculation requires the complete spectral information of a spectrophotometer. On the other hand, data for calculating the r/g ratio can be provided by the red and green channels of CCD cameras as well, and thus, the next sections will focus on this property only, targeting cheap and scalable future applications for biosensing. This detection method sacrifices the LOD with approximately 1 order of magnitude (see Fig. 5), but is supported also by the direct proportionality between the r/g and peak position values. According to the scaling relation a change of 0.1 in the r/g value corresponds to a wavelength shift of $\sim$7 nm in the peak position, a relation similar to those found in earlier works[25, 52].

3.3. Effect of salt on sensitivity and SNP detection

Lowering the electrostatic repulsion between nucleotide sequences by increasing the sodium salt concentration makes the capture probes more accessible for the targets and also increases the maximum number of capture probes single AuNPs can accommodate[51]. However, increasing the salt concentration above a certain limit causes the AuNPs themselves to aggregate as a result of highly decreased electrostatic repulsion between the particles, and as such, there is a salt concentration optimal for the assay. Fig. 5 shows the dose-response curves for targets with a gap of 4 bases (T4bp) and salt concentrations of 0.3 and 1 M. While the amplitude of the assay response for high analyte concentrations is higher in the case of 0.3 M salt, 1 M NaCl concentration results in lower LOD (see supporting information S2 for a close-up look) as well as in higher dynamic range. The results for targets with single nucleotide mismatching sequences (T4bp1MM) are also depicted in Fig. 5 for the two different salt concentrations. Investigating a sandwich assay similar to the one presented in this paper, a previous study has found the optimal salt concentration for discriminating the single-mismatched target (1MM) from the perfectly matched target (T) to be

0.25 M[53]. This is in accordance with our results, showing that the LOD for 1MM targets is higher for 0.3 M salt concentration. However, even in the case of 1 M NaCl concentration the assay is ∼3 orders of magnitude less sensitive for targets with single base mismatch. Due to the lower LOD and still high specificity, the next optimization steps presented in the following sections used 1 M NaCl concentration.

3.4. Effect of gap insertions in the target analyte sequence

As higher interparticle distance results in lower particle-to-particle repulsion and more stable dimer formation, it is interesting to study if introducing nonbase-paired gap regions in the analyte sequence, and as such increasing the interparticle distance, further improves the assay performance. On the other hand, increasing the distance between the particles reduces the plasmonic coupling that is expected to result in smaller signals and lower sensitivity. The results of studying this effect are presented in Fig. 6, showing that the sensitivity of the assay is indeed decreasing with increasing gap sizes, in agreement with previous studies on similar systems[49].

3.5. Effect of capture probe density

The last step of the assay optimization was varying the number of capture probes on the AuNPs. While higher capture probe densities could increase the sensitivity by increasing the probability of the binding events, at too high coverage fractions the accessibility of the capture probes becomes reduced due to overcrowding[54]. To study this effect equal fractions of A and B tails were systematically replaced by short poly-A sequences acting as lateral spacers, which simultaneously increased the accessibility and lowered the number of the capture probes. The resulting dose-response curves plotted in Fig. 7 show no significant difference between 100% and 75% capture probe densities, while 50% and 25% fractions lead to 3 and 5 orders of magnitude higher dissociation constants. The optimal capture probe density value close to 100% might originate from two reasons. Firstly, the curvature of the AuNP surfaces increases the accessibility of

capture probes compared to that on flat surfaces[55], and secondly, the 1 M salt concentration used for this set of experiments shields the repulsive forces between non-matching capture probe and analyte segments, again increasing the accessibility of the densely packed capture probes. Since the 100% and 75% assays show similar performances, the one with the maximal, 100% capture probe density was chosen as optimal due to its simplicity.

4. Conclusions

A simple, single-step, in solution method based on AuNP sandwich structures was developed and optimized for the quantification of short oligonucleotide sequences. The AuNP aggregation in the presence of target analytes was detected by darkfield spectroscopy. The optimization procedure has studied the effect of salt concentration, non-matching gap insertions, as well as capture probe density and found the assay having 1 M sodium salt concentration, fully base paired targets, and AuNPs with maximal capture probe density optimal. The optimized assay has a 1 fM LOD and fM to 10 pM dynamic range determined from the FWHM of the spectral response, while a much simpler method based on CCD detection increases the LOD by 1 order of magnitude with a dynamic range up to the nM range. The presented method is highly target specific as well, having 3–4 orders of magnitude higher LOD values for SNP detection. Comparison of the LOD and specificity achieved with those found in the literature is difficult due to the high diversity of target sequences and especially target lengths used to demonstrate the different methods, and often, SNP detection is demonstrated at selected target concentrations only. Nevertheless, optical, nanoparticle based biosensors for the detection of target analytes with similar lengths generally have LODs in the range of 1 fM – 10 pM, a dynamic range of 3–4 orders of magnitude in terms of target concentration, and target specificity down to 10 fM target concentrations[25, 37, 41, 45, 56–58].

Compared to the traditional methods, the simple, solution-based nature of the assay presented in this manuscript has improved performance by provid-

ing higher capture probe accessibility compared to flat surfaces, and since the method involves no washing steps also visualizes the possibility of faster, real-time read-outs of aggregated AuNPs right in their 3D environments. Together with the CCD detection method such a flexible, robust, and highly scalable sensing technology could lead to many new and improved oligonucleotide-sensing applications.

Acknowledgements

Financial support from ETH Zurich and the NCCR Molecular Systems Engineering is acknowledged.

Appendix A. Supplementary data

Supplementary material associated with this article can be found, in the online version, at ..

References

[1] F. S. Collins, Variations on a Theme: Cataloging Human DNA Sequence Variation, Science 278 (1997) 1580–1581. doi:10.1126/science.278.5343.1580.

[2] A. Falcón de Vargas, The Human Genome Project and its importance in clinical medicine (2002). doi:10.1016/S0531-5131(01)00570-2.

[3] A. L. Beaudet, J. W. Belmont, Array-based DNA diagnostics: let the revolution begin., Annual review of medicine 59 (2008) 113–129. doi:10.1146/annurev.med.59.012907.101800.

[4] P.-Y. Kwok, X. Chen, Detection of single nucleotide polymorphisms., Current issues in molecular biology 5 (2003) 43–60.

[5] G. C. Johnson, J. a. Todd, Strategies in complex disease mapping., Current opinion in genetics & development 10 (2000) 330–334.

[6] N. J. Risch, Searching for genetic determinants in the new millennium., Nature 405 (JUNE) (2000) 847–856. doi:10.1038/35015718.

[7] J. Perkel, SNP genotyping: six technologies that keyed a revolution, Nature Methods 5 (5) (2008) 447–453.
URL http://dx.doi.org/10.1038/nmeth0508-447

[8] R. Sachidanandam, D. Weissman, S. C. Schmidt, J. M. Kakol, L. D. Stein, G. Marth, S. Sherry, J. C. Mullikin, B. J. Mortimore, D. L. Willey, S. E. Hunt, C. G. Cole, P. C. Coggill, C. M. Rice, Z. Ning, J. Rogers, D. R. Bentley, P. Y. Kwok, E. R. Mardis, R. T. Yeh, B. Schultz, L. Cook, R. Davenport, M. Dante, L. Fulton, L. Hillier, R. H. Waterston, J. D. McPherson, B. Gilman, S. Schaffner, W. J. Van Etten, D. Reich, J. Higgins, M. J. Daly, B. Blumenstiel, J. Baldwin, N. Stange-Thomann, M. C. Zody, L. Linton, E. S. Lander, D. Altshuler, T. International, S. N. P. Map, W. Group, A map of human genome sequence variation containing 1.42 million single nucleotide polymorphisms., Nature 409 (February) (2001) 928–933. doi:10.1038/35057149.

[9] J. den Dunnen, S. Antonarakis, Nomenclature for the description of human sequence variations, Human Genetics 109 (1) (2014) 121–124.
URL http://link.springer.com/10.1007/s004390100505

[10] S. N. Silva, O. M. Gil, V. C. Oliveira, M. N. Cabral, A. P. Azevedo, A. Faber, I. Manita, T. C. Ferreira, E. Limbert, J. E. Pina, J. Rueff, J. Gaspar, Association of polymorphisms in ERCC2 gene with non-familial thyroid cancer risk., Cancer epidemiology, biomarkers & prevention : a publication of the American Association for Cancer Research, cosponsored by the American Society of Preventive Oncology 14 (10) (2005) 2407–12.
URL http://cebp.aacrjournals.org/content/14/10/2407

[11] G. Thomas, K. B. Jacobs, M. Yeager, P. Kraft, S. Wacholder, N. Orr, K. Yu, N. Chatterjee, R. Welch, A. Hutchinson, A. Crenshaw, G. Cancel-Tassin, B. J. Staats, Z. Wang, J. Gonzalez-Bosquet, J. Fang, X. Deng, S. I.

Berndt, E. E. Calle, H. S. Feigelson, M. J. Thun, C. Rodriguez, D. Albanes, J. Virtamo, S. Weinstein, F. R. Schumacher, E. Giovannucci, W. C. Willett, O. Cussenot, A. Valeri, G. L. Andriole, E. D. Crawford, M. Tucker, D. S. Gerhard, J. F. Fraumeni, R. Hoover, R. B. Hayes, D. J. Hunter, S. J. Chanock, Multiple loci identified in a genome-wide association study of prostate cancer., Nature genetics 40 (3) (2008) 310–5.
URL http://dx.doi.org/10.1038/ng.91

[12] R. A. Eeles, Z. Kote-Jarai, G. G. Giles, A. A. A. Olama, M. Guy, S. K. Jugurnauth, S. Mulholland, D. A. Leongamornlert, S. M. Edwards, J. Morrison, H. I. Field, M. C. Southey, G. Severi, J. L. Donovan, F. C. Hamdy, D. P. Dearnaley, K. R. Muir, C. Smith, M. Bagnato, A. T. Ardern-Jones, A. L. Hall, L. T. O'Brien, B. N. Gehr-Swain, R. A. Wilkinson, A. Cox, S. Lewis, P. M. Brown, S. G. Jhavar, M. Tymrakiewicz, A. Lophatananon, S. L. Bryant, A. Horwich, R. A. Huddart, V. S. Khoo, C. C. Parker, C. J. Woodhouse, A. Thompson, T. Christmas, C. Ogden, C. Fisher, C. Jamieson, C. S. Cooper, D. R. English, J. L. Hopper, D. E. Neal, D. F. Easton, Multiple newly identified loci associated with prostate cancer susceptibility., Nature genetics 40 (3) (2008) 316–21.
URL http://www.ncbi.nlm.nih.gov/pubmed/18264097

[13] F. K. Kavvoura, J. P. a. Ioannidis, CTLA-4 gene polymorphisms and susceptibility to type 1 diabetes mellitus: a HuGE Review and meta-analysis., American journal of epidemiology 162 (1) (2005) 3–16.
URL http://www.ncbi.nlm.nih.gov/pubmed/15961581

[14] Y.-J. Liu, X.-G. Liu, L. Wang, C. Dina, H. Yan, J.-F. Liu, S. Levy, C. J. Papasian, B. M. Drees, J. J. Hamilton, D. Meyre, J. Delplanque, Y.-F. Pei, L. Zhang, R. R. Recker, P. Froguel, H.-W. Deng, Genome-wide association scans identified CTNNBL1 as a novel gene for obesity., Human molecular genetics 17 (12) (2008) 1803–13.
URL http://www.pubmedcentral.nih.gov/articlerender.fcgi?artid=2900891&tool=pmcentrez&rendertype=abstract

[15] G. K. Geiss, R. E. Bumgarner, B. Birditt, T. Dahl, N. Dowidar, D. L. Dunaway, H. P. Fell, S. Ferree, R. D. George, T. Grogan, J. J. James, M. Maysuria, J. D. Mitton, P. Oliveri, J. L. Osborn, T. Peng, A. L. Ratcliffe, P. J. Webster, E. H. Davidson, L. Hood, K. Dimitrov, Direct multiplexed measurement of gene expression with color-coded probe pairs., Nature biotechnology 26 (3) (2008) 317–25.
URL http://dx.doi.org/10.1038/nbt1385

[16] Y. Yang, L. Zhao, Sensitive fluorescent sensing for DNA assay, TrAC - Trends in Analytical Chemistry 29 (9) (2010) 980–1003. doi:10.1016/j.trac.2010.05.009.
URL http://dx.doi.org/10.1016/j.trac.2010.05.009

[17] M.-L. Lunn, P. Mouritzen, K. Faber, N. Jacobsen, Micro RNA quantitation from a single cell by PCR using SYBR Green detection and LNA-bases primers, Nature Methods 4 (2) (2008) 24–25.
URL file:///D:/DatosdeUsuario/UJA/Misdocumentos/Bibliografia/Lunnetal.-2008-MicroRNAquantitationfromasinglecellbyPCRusingSYBRGreendetectionandLNA-bas
pdf

[18] C. M. Hindson, J. R. Chevillet, H. A. Briggs, E. N. Gallichotte, I. K. Ruf, B. J. Hindson, R. L. Vessella, M. Tewari, Absolute quantification by droplet digital PCR versus analog real-time PCR., Nature methods 10 (10) (2013) 1003–5.
URL http://dx.doi.org/10.1038/nmeth.2633

[19] F. V. Wintzingerode, U. B. Göbel, E. Stackebrandt, Determination of microbial diversity in environmental samples: Pitfalls of PCR-based rRNA analysis, FEMS Microbiology Reviews 21 (1997) 213–229. doi:10.1016/S0168-6445(97)00057-0.

[20] D. Klein, Quantification using real-time PCR technology: Applications and limitations, Trends in Molecular Medicine 8 (6) (2002) 257–260. doi:10.1016/S1471-4914(02)02355-9.

[21] C. J. Smith, a. M. Osborn, Advantages and limitations of quantitative PCR (Q-PCR)-based approaches in microbial ecology, FEMS Microbiology Ecology 67 (1991) (2009) 6–20. doi:10.1111/j.1574-6941.2008.00629.x.

[22] L. Garibyan, N. Avashia, Polymerase Chain Reaction, Journal of Investigative Dermatology 133.

[23] Y. Sohni, S. Kanjilal, V. Kapur, Performance evaluation of five commercial real-time PCR reagent systems using TaqMan assays for B. anthracis detection., Clinical biochemistry 41 (7-8) (2008) 640–4.
URL http://www.scopus.com/inward/record.url?eid=2-s2.0-41849083022&partnerID=tZOtx3y1

[24] J.-M. Nam, S. I. Stoeva, C. A. Mirkin, Bio-bar-code-based DNA detection with PCR-like sensitivity., Journal of the American Chemical Society 126 (19) (2004) 5932–3.
URL http://www.scopus.com/inward/record.url?eid=2-s2.0-2442575025&partnerID=tZOtx3y1

[25] R. Verdoold, R. Gill, F. Ungureanu, R. Molenaar, R. P. H. Kooyman, Femtomolar DNA detection by parallel colorimetric darkfield microscopy of functionalized gold nanoparticles., Biosensors & bioelectronics 27 (1) (2011) 77–81.
URL http://www.ncbi.nlm.nih.gov/pubmed/21752628

[26] N. G. Khlebtsov, L. A. Dykman, Optical properties and biomedical applications of plasmonic nanoparticles, Journal of Quantitative Spectroscopy and Radiative Transfer 111 (1) (2010) 1–35.
URL http://www.sciencedirect.com/science/article/pii/S0022407309002581

[27] X. Huang, M. a. El-Sayed, Gold nanoparticles: Optical properties and implementations in cancer diagnosis and photothermal therapy, Journal of

Advanced Research 1 (1) (2010) 13–28.
URL http://linkinghub.elsevier.com/retrieve/pii/S2090123210000056

[28] C. a. Mirkin, R. L. Letsinger, R. C. Mucic, J. J. Storhoff, A DNA-based method for rationally assembling nanoparticles into macroscopic materials. (1996). doi:10.1038/382607a0.

[29] R. Elghanian, Selective Colorimetric Detection of Polynucleotides Based on the Distance-Dependent Optical Properties of Gold Nanoparticles, Science 277 (5329) (1997) 1078–1081.
URL http://www.sciencemag.org/cgi/doi/10.1126/science.277.5329.1078

[30] J. J. Storhoff, R. Elghanian, R. C. Mucic, C. A. Mirkin, R. L. Letsinger, One-pot colorimetric differentiation of polynucleotides with single base imperfections using gold nanoparticle probes, Journal of the American Chemical Society 120 (97) (1998) 1959–1964. doi:10.1021/ja972332i.

[31] D. S. Seferos, D. A. Giljohann, H. D. Hill, A. E. Prigodich, C. A. Mirkin, Nano-flares: probes for transfection and mRNA detection in living cells., Journal of the American Chemical Society 129 (50) (2007) 15477–9.
URL http://www.pubmedcentral.nih.gov/articlerender.fcgi?artid=3200543&tool=pmcentrez&rendertype=abstract

[32] F. Vollmer, S. Arnold, D. Braun, I. Teraoka, A. Libchaber, Multiplexed DNA quantification by spectroscopic shift of two microsphere cavities., Biophysical journal 85 (3) (2003) 1974–9.
URL http://www.pubmedcentral.nih.gov/articlerender.fcgi?artid=1303369&tool=pmcentrez&rendertype=abstract

[33] J. J. Storhoff, A. D. Lucas, V. Garimella, Y. P. Bao, U. R. Müller, Homogeneous detection of unamplified genomic DNA sequences based on colorimetric scatter of gold nanoparticle probes., Nature biotechnology 22 (7) (2004) 883–887. doi:10.1038/nbt977.

[34] P. Baptista, G. Doria, D. Henriques, E. Pereira, R. Franco, Colorimetric detection of eukaryotic gene expression with DNA-derivatized gold nanoparticles, Journal of Biotechnology 119 (2005) 111–117. doi:10.1016/j.jbiotec.2005.02.019.

[35] I. Bernacka-Wojcik, H. Águas, F. F. Carlos, P. Lopes, P. J. Wojcik, M. N. Costa, B. Veigas, R. Igreja, E. Fortunato, P. V. Baptista, R. Martins, Single nucleotide polymorphism detection using gold nanoprobes and biomicrofluidic platform with embedded microlenses, Biotechnology and Bioengineering 9999 (xxx) (2015) n/a–n/a. doi:10.1002/bit.25542.
URL http://doi.wiley.com/10.1002/bit.25542

[36] T. Sannomiya, C. Hafner, J. Voros, In situ sensing of single binding events by localized surface plasmon resonance., Nano letters 8 (10) (2008) 3450–5.
URL http://dx.doi.org/10.1021/nl802317d

[37] Z. Yuan, J. Cheng, X. Cheng, Y. He, E. S. Yeung, Highly sensitive DNA hybridization detection with single nanoparticle flash-lamp darkfield microscopy, The Analyst 137 (13) (2012) 2930. doi:10.1039/c2an16171k.

[38] J. J. Storhoff, S. S. Marla, P. Bao, S. Hagenow, H. Mehta, A. Lucas, V. Garimella, T. Patno, W. Buckingham, W. Cork, U. R. Müller, Gold nanoparticle-based detection of genomic DNA targets on microarrays using a novel optical detection system, Biosensors and Bioelectronics 19 (8) (2004) 875–883. doi:10.1016/j.bios.2003.08.014.

[39] G. Doria, R. Franco, P. Baptista, Nanodiagnostics : fast colorimetric method for single nucleotide polymorphism / mutation detection, IET Nanobiotechnol 1 (4) (2007) 53–57. doi:10.1049/iet-nbt.

[40] F. F. Carlos, O. Flores, G. Doria, P. V. Baptista, Characterization of genomic single nucleotide polymorphism via colorimetric detection using a single gold nanoprobe, Analytical Biochemistry 465 (2014) 1–5. doi:10.1016/j.ab.2014.07.019.

URL http://linkinghub.elsevier.com/retrieve/pii/S0003269714003133

[41] W. J. Yang, X. B. Li, Y. Y. Li, L. F. Zhao, W. L. He, Y. Q. Gao, Y. J. Wan, W. Xia, T. Chen, H. Zheng, M. Li, S. Q. Xu, Quantification of microRNA by gold nanoparticle probes, Analytical Biochemistry 376 (2) (2008) 183–188. doi:10.1016/j.ab.2008.02.003.

[42] Y. Ding, Z. Jiang, K. Saha, C. S. Kim, S. T. Kim, R. F. Landis, V. M. Rotello, Gold nanoparticles for nucleic acid delivery., Molecular therapy : the journal of the American Society of Gene Therapy 22 (6) (2014) 1075–83.
URL http://dx.doi.org/10.1038/mt.2014.30

[43] X.-Y. Wan, L.-L. Zheng, P.-F. Gao, X.-X. Yang, C.-M. Li, Y. F. Li, C. Z. Huang, Real-time light scattering tracking of gold nanoparticles-bioconjugated respiratory syncytial virus infecting HEp-2 cells., Scientific reports 4 (2014) 4529.
URL http://www.pubmedcentral.nih.gov/articlerender.fcgi?artid=3970125&tool=pmcentrez&rendertype=abstract

[44] C.-W. Lee, M. J. Chen, J.-Y. Cheng, P.-K. Wei, Morphological studies of living cells using gold nanoparticles and dark-field optical section microscopy., Journal of biomedical optics 14 (3) (2014) 034016.
URL http://www.ncbi.nlm.nih.gov/pubmed/19566309

[45] M. S. Cordray, M. Amdahl, R. R. Richards-Kortum, Gold nanoparticle aggregation for quantification of oligonucleotides: Optimization and increased dynamic range, Analytical Biochemistry 431 (2) (2012) 99–105. doi:10.1016/j.ab.2012.09.013.
URL http://dx.doi.org/10.1016/j.ab.2012.09.013

[46] S. J. Park, A. a. Lazarides, J. J. Storhoff, L. Pesce, C. a. Mirkin, The structural characterization of oligonucleotide-modified gold nanoparticle

networks formed by DNA hybridization, Journal of Physical Chemistry B 108 (2004) 12375–12380. doi:10.1021/jp040242b.

[47] R. A. Reynolds, C. A. Mirkin, R. L. Letsinger, Homogeneous, nanoparticle-based quantitative colorimetric detection of oligonucleotides [13], Journal of the American Chemical Society 122 (15) (2000) 3795–3796. doi:10.1021/ja000133k.

[48] O.-S. Lee, T. R. Prytkova, G. C. Schatz, Using DNA to Link Gold Nanoparticles, Polymers and Molecules: a Theoretical Perspective., The journal of physical chemistry letters 1 (12) (2010) 1781–1788.
URL http://www.pubmedcentral.nih.gov/articlerender.fcgi?artid=2893743&tool=pmcentrez&rendertype=abstract

[49] B. D. Smith, N. Dave, P.-J. J. J. Huang, J. Liu, Assembly of DNA-functionalized gold nanoparticles with gaps and overhangs in linker DNA, Journal of Physical Chemistry C 115 (16) (2011) 7851–7857. doi:10.1021/jp111073w.
URL http://pubs.acs.org/doi/abs/10.1021/jp111073w

[50] B.-A. Du, Z.-P. Li, C.-H. Liu, One-step homogeneous detection of DNA hybridization with gold nanoparticle probes by using a linear light-scattering technique., Angewandte Chemie (International ed. in English) 45 (47) (2006) 8022–5.
URL http://www.ncbi.nlm.nih.gov/pubmed/17091512

[51] S. J. Hurst, A. K. R. Lytton-Jean, C. a. Mirkin, Maximizing DNA loading on a range of gold nanoparticle sizes, Analytical Chemistry 78 (24) (2006) 8313–8318. doi:10.1021/ac0613582.

[52] F. Ungureanu, D. Wasserberg, N. Yang, R. Verdoold, R. P. H. Kooyman, Immunosensing by colorimetric darkfield microscopy of individual gold nanoparticle-conjugates, Sensors and Actuators, B: Chemical 150 (2) (2010) 529–536. doi:10.1016/j.snb.2010.08.044.
URL http://dx.doi.org/10.1016/j.snb.2010.08.044

[53] Z. Zhan, X. Ma, C. Cao, S. J. Sim, Gold-based optical biosensor for single-mismatched DNA detection using salt-induced hybridization., Biosensors & bioelectronics 32 (1) (2012) 127–32.
URL http://www.sciencedirect.com/science/article/pii/S0956566311007895

[54] A. W. Peterson, The effect of surface probe density on DNA hybridization, Nucleic Acids Research 29 (24) (2001) 5163–5168.
URL http://nar.oxfordjournals.org/content/29/24/5163.full

[55] H. D. Hill, J. E. Millstone, M. J. Banholzer, C. a. Mirkin, The role radius of curvature plays in thiolated oligonucleotide loading on gold nanoparticles, ACS Nano 3 (2) (2009) 418–424. doi:10.1021/nn800726e.

[56] X. Yao, X. Li, F. Toledo, C. Zurita-Lopez, M. Gutova, J. Momand, F. Zhou, Sub-attomole oligonucleotide and p53 cDNA determinations via a high-resolution surface plasmon resonance combined with oligonucleotide-capped gold nanoparticle signal amplification, Analytical Biochemistry 354 (2) (2006) 220–228. doi:10.1016/j.ab.2006.04.011.

[57] R. D'Agata, R. Corradini, G. Grasso, R. Marchelli, G. Spoto, Ultrasensitive detection of DNA by PNA and nanoparticle-enhanced surface plasmon resonance imaging, ChemBioChem 9 (13) (2008) 2067–2070. doi:10.1002/cbic.200800310.

[58] S. K. Kim, H. Cho, J. Jeong, J. N. Kwon, Y. Jung, B. H. Chung, Label-free and naked eye detection of PNA/DNA hybridization using enhancement of gold nanoparticles., Chemical communications (Cambridge, England) 46 (19) (2010) 3315–3317. doi:10.1039/b926940a.

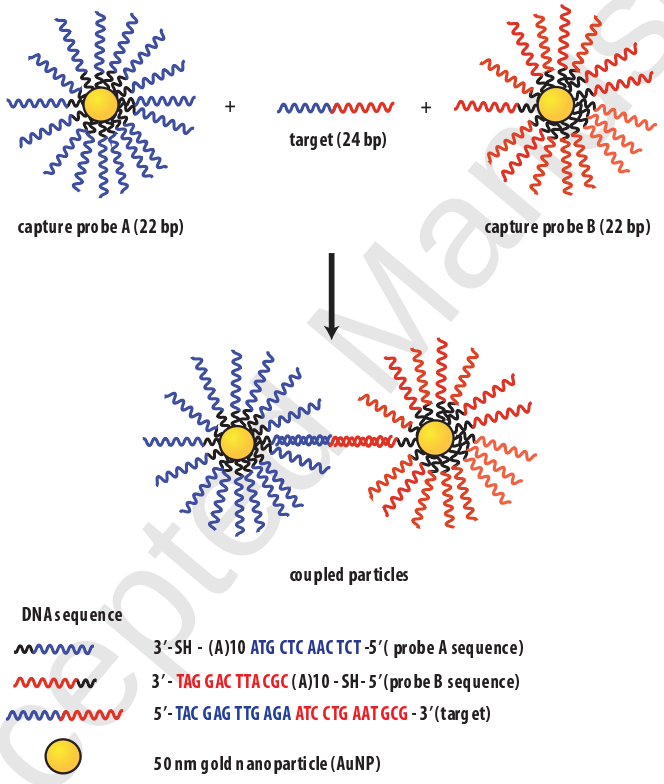

Figure 1: Schematics of the assay. The target DNA (T) half-complementary to capture probes A and B is binding the two AuNPs together to form a sandwich structure by hybridization.

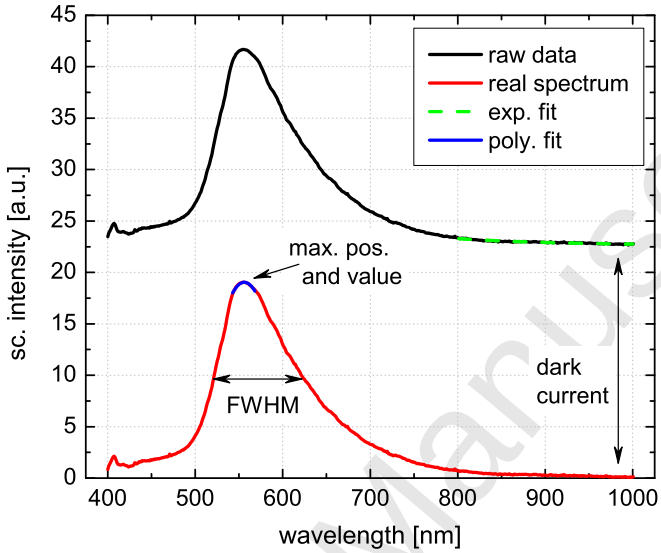

Figure 2: Baseline removal from a raw spectrum (black curve) to obtain the real spectrum (shown in red). Maximum position, maximum value, and full width at half maximum (FWHM) of the average scattered signal were calculated by fitting a second-order polynomial function (blue continuous curve) to the maximum and its 30 nm vicinity of the curve.

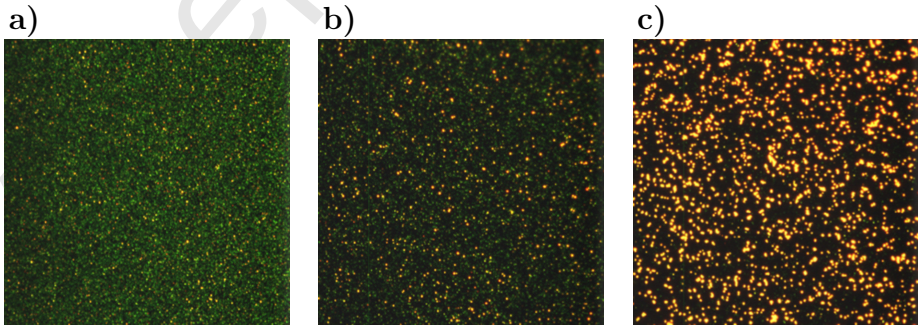

Figure 3: Typical darkfield images of the 150 μm $\times$ 150 μm scanning area with increasing analyte concentrations of 0M (a), 0.1 pM (b), and 1 μM (c).

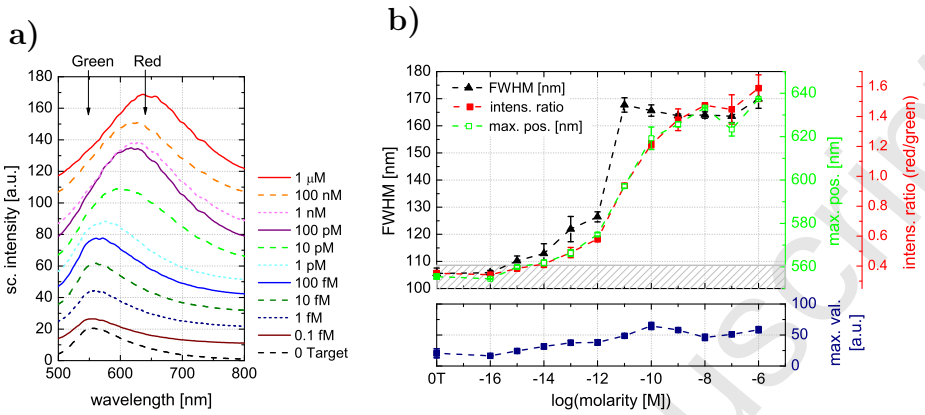

Figure 4: Analysis of a set of experiments to calculate the dose-response curve in the case of the optimized assay. a) The calculated real spectra at increasing target concentrations. The spectral curves were shifted incrementally by 10 a.u. on the intensity axis for better visibility. 'Red' and 'Green' mark the wavelengths for the r/g analysis (see corresponding text for details). b) Dose-response curves calculated from the different spectral properties. '0T' represents the samples with zero target concentration, the shaded area the LOD calculated from the FWHM values, while dashed curves serve as visual guides only. The error bars give the standard deviation of measurements made on three independent samples from the same assay preparation.

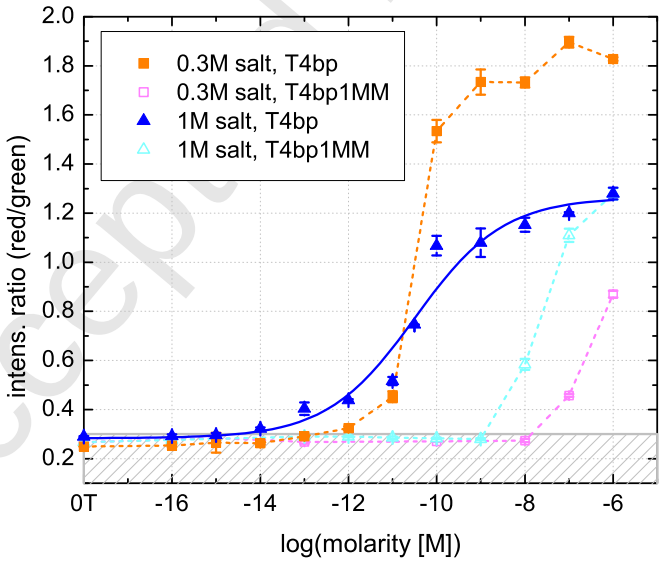

Figure 5: The effect of hybridization buffer salt concentration on the sensitivity and SNP detection. T4bp and T4bp1MM are targets with a gap of 4 bases and having complementary and single nucleotide mismatching sequences, respectively. The solid curve and shaded area are the result of a sigmoidal fit and indication of the LOD, respectively, in the case of T4bp and 1 M salt concentration, while dashed curves serve as visual guides only. '0T' represents the samples with zero target concentration. The error bars give the standard deviation of measurements made on three independent samples from the same assay preparation.

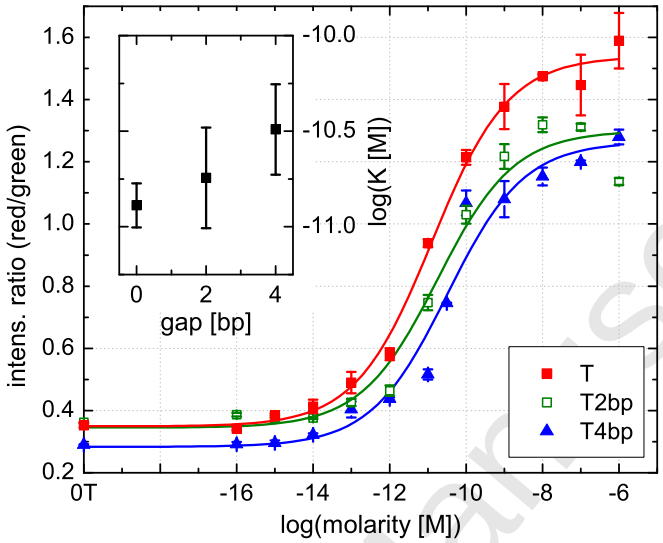

Figure 6: The effect of gap insertions in the target analyte sequence. T indicates the fully base paired target with no gaps, while T2bp, and T4bp are targets with nonbase-paired regions of 2 and 4 bases, respectively. Solid curves are sigmoidal fits based on which the dissociation constants plotted in the inset are determined. '0T' represents the samples with zero target concentration. The error bars give the standard deviation of measurements made on three independent samples from the same assay preparation.

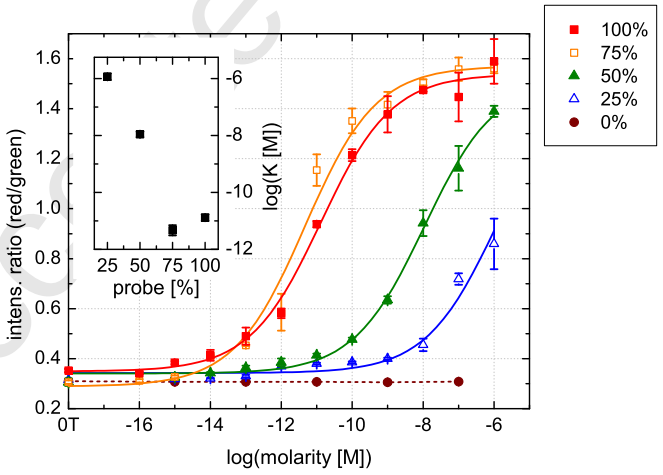

Figure 7: The effect of capture probe density of AuNPs. The presented percentage values correspond to the ratio of capture probes not replaced by short poly-A sequences acting as spacers. Curves are sigmoidal fits based on which the dissociation constants plotted in the inset are determined. '0T' represents the samples with zero target concentration. The error bars give the standard deviation of measurements made on three independent samples from the same assay preparation.

Femtomolar oligonucleotide detection by a one-step gold nanoparticle-based assay

Highlights

- A one-step, solution-based assay for oligonucleotide detection is shown.
- The optimization process for the highest assay sensitivity is presented.
- The optimized assay has a 1 fM limit of detection and fM to 10 pM dynamic range.
- The simple, CCD-based detection provides 10 fM LOD with a dynamic range up to nM.
- The method is also suitable for SNP detection.

Femtomolar oligonucleotide detection by a one-step gold nanoparticle-based assay

Caption for the graphical abstract

This work presents a single-step, sequence-specific oligonucleotide detection method based on tail-to-tail aggregation of functionalized gold nanoparticles in the presence of target analytes. Using cost-effective instrumentation and the corresponding simplified analysis, the optimized assay has a 10 fM limit of detection and dynamic range up to nM analyte concentration. The detection of perfect match sequences were 3 orders of magnitude more sensitive than targets with single nucleotide mismatches.